Optimising Hard X-ray Generation from Laser-Produced Plasmas

Diploma work
by
Christofer Lindheimer F-89
LRAP-162
Lund, April 1995

Abstract

The aim of this work is to increase the X-ray yield for a laser produced plasma by optimising the focusing conditions and temporal shape of the laser pulses.
The focusing conditions are improved by introducing a control system that secures the laser target surface to exact focus within a range of a few micrometers, allowing continuously high laser intensity for plasma generation.
The temporal shape of the laser pulses is changed by introducing a saturable absorber in the laser beam. The laser produces a substantial pre-pulse that heats and expands the target material prior to main pulse arrival. The saturable absorber can increase the main pulse/pre-pulse ratio of the laser pulse up to four orders of magnitude and consequently reduce expansion of the target material before the main pulse. The belief is that an increase in target density at the time of main pulse arrival will change the energy distribution of the X-rays, towards a more efficient X-ray production in the hard X-ray region.
This report and the work connected to it, includes the preliminary measurements and results for these improvements.

Contents Page

1. Introduction

When sub-picosecond pulses from a high power laser are focused onto a solid target with a high atomic number, a radiating plasma is created. This plasma emits intense radiation in a large spectral range, from the soft up to the hard X-ray region, in excess of 1 MeV [1]. The radiation can be used for imaging and, hopefully, in a near future, medical applications with these X-rays will become possible. The resolution in imaging is much higher than for conventional X-ray tubes because the radiation source is extremely small. Magnification imaging is tried and shown to be successful in up to 80 times magnification [1]. Clearly, there are advantages by using this technique in medical imaging, instead of X-ray tubes, if it is shown to be harmless for living tissue.
This diploma work, contains a study of optimisations of the generation of hard X-rays, along *two* lines.

1. The focusing of the laser requires the target position to be accurate within a few micrometers, in order to maintain a high laser intensity for plasma generation. Problems arise because a moving target is needed, to ensure focusing of the laser pulses onto a fresh spot of the target material for each new shot. When a circular foil of the target material rotates, a wobble connected with this rotation, shifts the position of the plate, so the focus is sometimes in front of or behind the target surface. ***Position control*** for these movements is developed, with a commercial PID controller and a low-pass filtering of the position signal, rejecting position changes with frequencies higher than 1 Hz. The filtering is introduced to exclude control of electrical and optical noise and in this first attempt, control of high-frequency position changes is neglected.

2. The laser produces pulses of sub-picosecond duration. Before the main pulse, a pre-pulse, 5-6 orders of magnitude smaller, is generated. If this is intense enough, it can spoil the high-density plasma by pre-ionising the target. This will result in a target expansion and a decrease in target density, before the main pulse arrives. A ***saturable absorber*** is introduced in the laser beam, which allows a change of the main pulse/pre-pulse ratio by up to four orders of magnitude. The ability to change the main pulse/pre-pulse ratio makes it possible to detect the importance of a pre-pulse. By altering the saturation level of the absorber, it is possible to find the conditions for optimised X-ray generation. This does not necessarily have to be the highest main pulse/pre-pulse ratio.

The following chapter will shortly present the theory behind laser-produced plasma in general. Thereafter, the results of the experiments done on these two projects will be presented as well as two smaller changes in the experimental set-up.

2. Generation of X-rays from Laser-Produced Plasmas

2.1 X-ray radiating plasma generation

Generating X-rays with a pulsed laser is possible on any matter if the focal intensity is greater than 10^{11} W/cm^2 for a nanosecond pulse [2]. For higher intensities, higher temperatures are obtained and thus shorter wavelengths for the emitted X-rays. In this experiment, sub-picosecond pulses with intensities greater than 10^{18} W/cm^2 are used and enables production of MeV X-rays.

The extremely high intensities and the ultrafast pulses used here opens up a new field in plasma physics where the physical processes that occur in the creation of MeV X-rays are still unknown. However, the *known* processes that occur in a laser-produced plasma are still important since it is the origin of less energetic X-rays.

If a high power laser pulse (nanosecond pulse) is focused on a solid target, the surface ionises and vaporises. This is a result of interaction between the electromagnetic field in the laser light and the electrons in the target material. The material propagates away from the surface and the ablation creates a low-density region in which many plasma processes occur. When the thin plasma layer exists, the incoming laser radiation is absorbed by *inverse Bremstrahlung* in this low-density layer. This is a process in which a photon is absorbed by an ion-electron system and the electron is raised from a lower to a higher energy level. The electrons in the laser beam that are driven by the laser field acquire a kinetic energy that can heat the plasma when it is converted to thermal energy through collisions between ions and electrons.

If very short pulses (sub-picosecond pulses), created by a terawatt laser system, are fired onto the target, the plasma does not have time to expand and the laser plasma processes must occur in the full (or almost full) density of the target. Rapid collisional effects will insure both fast heating and fast cooling and consequently, the produced X-rays can be very bright and short lived. The adiabatic expansion also contributes to the fast cooling.

For this experiment, however, the laser produces a substantial prepulse that will reach the target 11 ns before the main pulse. During this time, the target surface can ablate and the high-density interactions will be lost. The prepulse interaction will yield the low-density region mentioned above. The main laser pulse propagates through the pre-pulse plasma region until it reaches the *critical density* for the laser frequency.

$$n_{cr} = \frac{m_e \varepsilon_0 {\omega_L}^2}{e^2} \qquad (2.1)$$

(m_e = electron mass ω_L = laser frequency)

The laser pulse can interact with the plasma prior to this point as a travelling wave. At the critical density, the light wave will be reflected. Estimates of the *inverse Bremstrahlung* heating effect reveal that it can raise the temperature to about 1 keV in the low-density region. To obtain MeV electrons, however, non-thermal processes are suggested to play a significant role [2].

A number of non-collisional processes are known for laser-plasma interactions. These are for example stimulated Raman scattering, stimulated Brillouin scattering and

resonance absorption. The result of each of these processes is to create a large amplitude plasma wave near the critical density. The plasma wave is the collective oscillation of the electrons with respect to the ions, that occurs at the plasma frequency [3], ω_P ;

$$\omega_P = \left(\frac{n_e e^2}{m_e \varepsilon_0} \right)^{1/2} \qquad (2.2)$$

(same relation as 2.1, but for the plasma frequency)
where n_e is the electron density. This characteristic frequency determines the response to radiation incident on the plasma [3]. If the incident frequency matches the plasma frequency, a resonance interaction may occur and the transfer of energy from the electromagnetic wave to the plasma may be greatly enhanced. The plasma wave can then accelerate electrons to very high energies. The energy extraction from this plasma wave is called *Landau damping*, [4]. Descriptively, what happens is that a cold electron is accelerated to a near-relativistic velocity within 1/2 cycle of the plasma wave. Any electron in the vicinity of the wave will be accelerated into a trajectory that will continue to allow it to extract energy from the wave. If enough acceleration is given to the electron during the first 1/2 cycle, such that the electron velocity is comparable to the plasma wave velocity, then it can stay phased and continue to extract energy, as it moves with the wave, like a surfer gains energy from a water wave. This region is often called non-linear Landau damping [5] and is suggested [2] to play an important role in the creation of MeV electrons.

For the emitted X-rays from the plasma, there are a few features well worth mentioning here:
The spectral distribution of the X-rays is measured in earlier experiments, [2], and do not seem to depend on the target atomic number. Except for the position of the characteristic peaks, which is directly proportional to the atomic number of the target, only the yield shows significant variation (above 20 keV). The characteristic peaks are related to the atomic number, Z as:

$$1/\sqrt{\lambda} = C(Z - \sigma) \qquad (2.3)$$

where C and σ are constants characterising a particular spectral series and λ is the wavelength. This is called *Moseley's law.*
The average X-ray yield increases as the 3/2 power of the incident laser energy, so increasing the energy will show a greater conversion. (At present, the conversion is estimated to be less than 1% for X-rays between 20 keV and 1 MeV. Earlier estimation is 0.3 %, [2], with a laser of three times less power than the one used here.)

2.2 The Laser System

The laser system used to generate an X-ray emitting plasma is a terawatt laser based on chirped pulse amplification [6]. This is a technique to achieve very high intensities in a small and compact laser system. The idea is to stretch the pulse in time before amplification, and then to compress it again, after the final amplifier. This allows a low peak power in the amplifying stage. The system is running at 10 Hz and it generates tuneable radiation in 760-840 nm region. The maximum power is 1.5 TW and the pulselength is 150 fs.

2.3 Experimental set-up

The experiment chamber is shown in figure 2.1. It consists of a vacuum chamber, a target and a focusing mirror. The laser light it focused onto the target by a gold-coated off-axis parabolic mirror. The generated X-rays exit the chamber through a thin plastic film, which is thick enough not to break under the vacuum pressure. A glass window is used to let the laser light through into the chamber. When running the experiment, the whole set-up is enclosed in lead-brick shielding to protect personnel in the surrounding area from X-rays. The target is a thin (0.25 mm) tantalum or gadolinium foil, mounted on a DC-motor driven rotating steel disc. The electric equipment to control this motor, as well as translation control for the target, is connected with vacuum-tight electrical feed throughs to the outside of the chamber. A pressure of 20-30 Torr is maintained in the chamber when running the experiment, to help prevent the target material from coating the optics. This is because tantalum (or gadolinium) forms a sputtering dust when the plasma forms. The laser is running at a wavelength of 794 nm with an energy of <350 mJ before compression. This corresponds to <150 mJ in the output pulse.

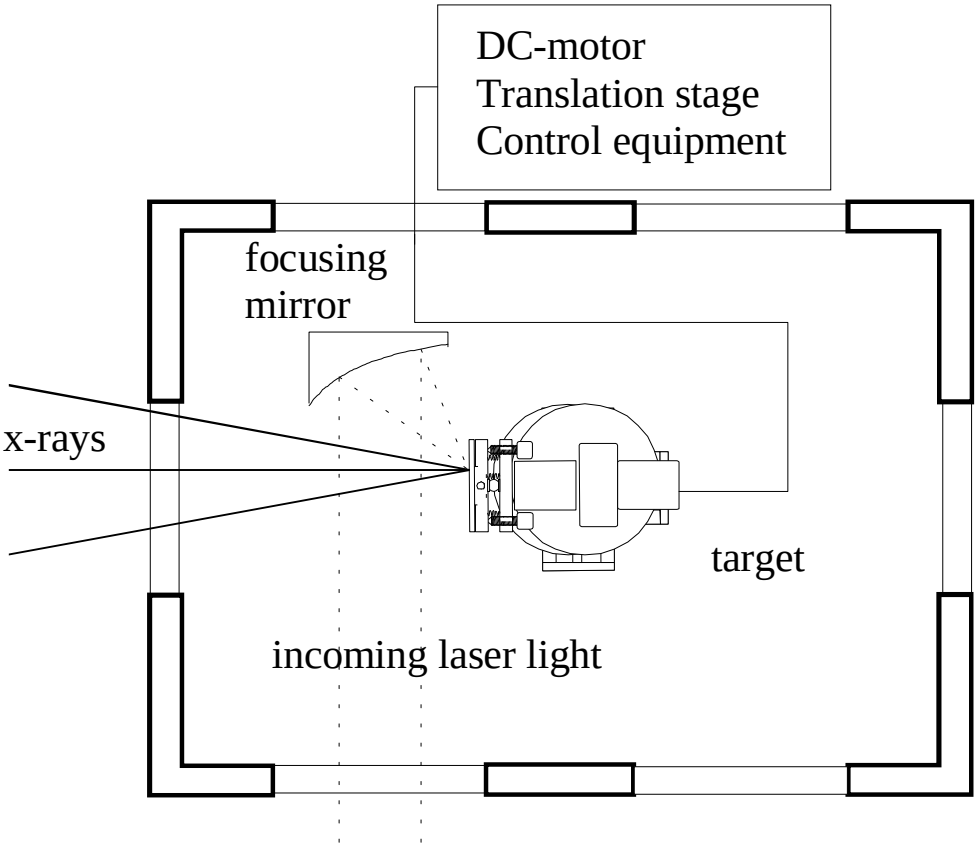

Figure 2.1: The experiment chamber for generating X-rays

3. Position control of the target

3.1 Introduction to position control

A thin foil of tantalum (Ta) or gadolinium (Gd) is used as a target for the terawatt laser pulses. The foil is mounted on a rotating disc. Rotations are introduced to avoid focusing on the same spot repetitively, since the pulses make small holes in the material, i.e. it destroys the material.
A high laser intensity is one of the most important factors for good X-ray generation. This makes it crucial that the focusing on the target is accurate, that is, that the exact focus position really is **on** the target surface. The exact focus is found by looking at the visible light that also is produced when plasma forms. An extremely hot plasma (good focusing) emits white light [2] while out-of-focus plasma radiates green or blue light. The blue light originates from the second harmonic of the incident laser and the green light from the 3/2 harmonic.
Rotating the target introduces problems, concerning the accuracy of focusing. All rotations suffer from wobbling of some magnitude if the rotating object is not mounted exactly perpendicular to the rotating axis. This will ruin the good focusing and by that, also the hot plasma formation. Another source for movements is that the mounting of the target foil may contribute to an uneven target surface. The foil is glued onto a steel disc and if it is applied unevenly, it can result in small irregularities in the surface. The partial heating of the target when focusing the laser on it, induces expansion that can result in production of undesired target movements. The facts mentioned, adding that the target surface only is prepared to be shiny with a machine shop buffing wheel, makes it possible to differ three sources of movements. These movements are listed in decreasing order in table 3.1.

Sources of position changes	Estimated Movements (μm)
1. Mechanical Wobble (manually adjusted)	>10
2. Coarseness from glue and heating	<10
3. Surface polish	not estimated

Table 3.1 Different sources of position changes and estimated magnitudes

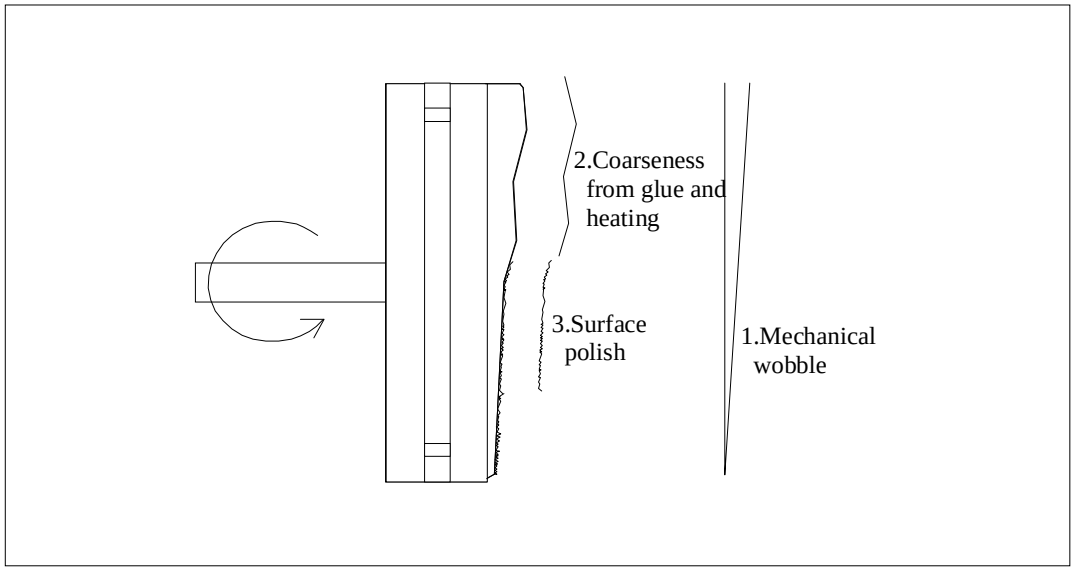

Figure 3.1: The target and different sources of wobble (overdone for clarity)

The desired accuracy is determined by the *confocal parameter* for Gaussian beams [7]. This is a measure of how far from the exact focus position (beam waist) the diameter of the laser beam is a factor $2^{1/2}$ larger than the actual beam waist. At this position, the intensity has changed a factor 1/2. The focal spotsize is on the order of a few μm and the confocal parameter about the same, so this implies that control in the same range is needed. The surface polish induced position changes is not important in this first attempt of position control because the revolution speed of the target (≈20 seconds) makes this a high-frequency change. The reason high-frequency changes should be neglected, is that it is not (yet) possible to measure the position in the same spot on the target as the terawatt laser pulses are focused. Fast changes that occur at a distance from the terawatt focus are more of a nuisance and therefore neglected.
For the previous experiments, with this type of target, only a manual adjustment was conducted to minimise the wobble. The disc with the target foil is mounted on another plate with two adjusting screws, a steel ball and springs**,** allowing manual setting down to 10 μm accuracy. However, during experiments, readjustments are constantly required in order to get a good plasma. These readjustments are hard to do by hand, and a control equipment is needed, to bring the movements down to the desired accuracy. With a piezo-translation stage, it is possible to control the target position by connecting it to a PID controller (**P**roportional, **I**ntegrating, **D**ifferential), that feeds it with a signal and thus translates the target. Detecting the position, a position sensitive diode, PSD, is used together with a HeNe-laser. By focusing the laser onto the target at an angle, a target movement back or forth will make the focus spot move sideways, see figure 3.2. If the spot is re-imaged onto the PSD at the angle of the reflected light, these movements occur in the image as well, and can then be detected. It is possible to resolve movements down to μm-accuracy.
In the following sub-chapters, a description of the experimental set-up will be presented. This is followed by a report of the results achieved for the measurements.

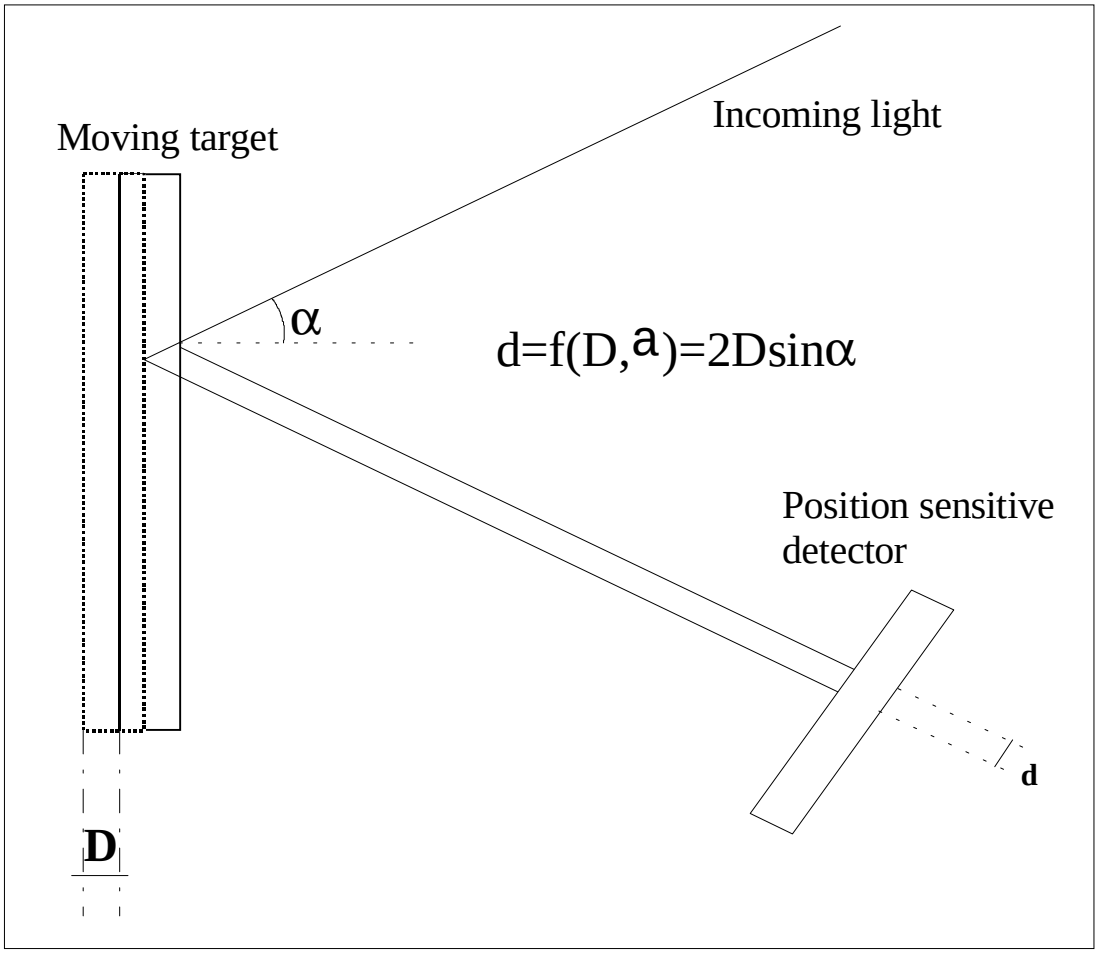

Figure 3.2: Position movements detected by the PSD (Position Sensitive Detector)
The distance d is determined as:

$a = \frac{D}{\cos\alpha}$ *and* $2a\sin\alpha = d'$ *, which gives*

$d = d'\cos\alpha$ *and thus the expression for d in D becomes*

$$d = \frac{2D\sin\alpha\cos\alpha}{\cos\alpha} = 2D\sin\alpha$$

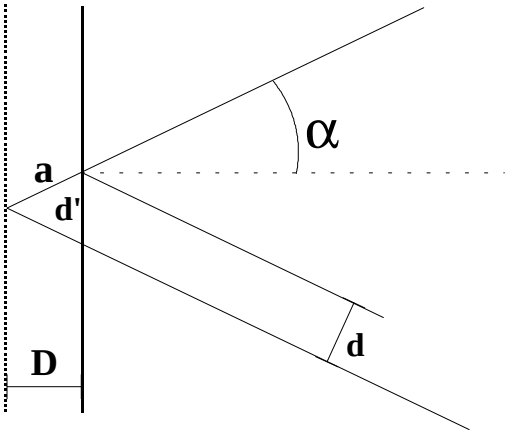

The angle α in the experimental set-up is about 20 degrees.

3.2 The equipment

The experimental set-up for position control in an environment outside the experimental chamber used for X-ray generation is shown in figure 3.3. A beam-expanded HeNe-laser is focused on the target. The focus is then re-imaged onto the PSD by collecting the reflected light with a lens. The signal from the PSD feeds a PID controller, which gives a signal to a piezo-translation stage to move the target backwards or forwards, to get it back in exact focus position. The position changes are registered by a plotter.

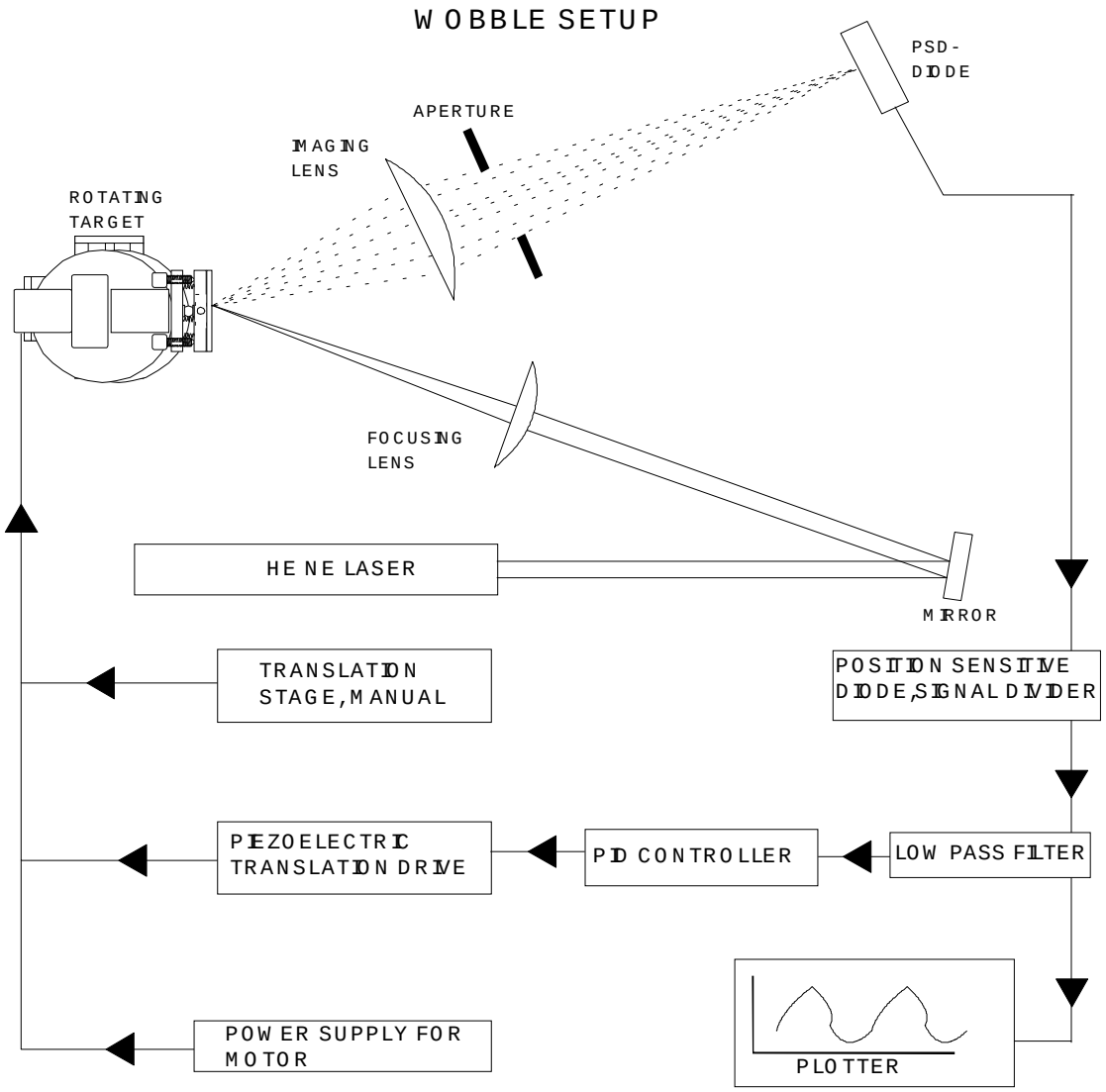

Figure 3.3: Set-up for position measurement and control.

3.2.1 The Position Sensitive Diode, PSD

The device generating a position signal is shown in figure 3.4. It is a Hamamatsu S3931 one-dimensional position sensitive diode with a sensitive area of 1×6 mm and a rise time of 1.5 μs. The position resolution is 0.2 μm and the wavelength range is 320-1100 nm. The construction of the diode is such that when a light spot falls on it, an electric charge proportional to the light energy is generated at the incident position. This charge is driven through a resistive P-layer and collected by two electrodes, one at each end of the diode. The resistivity of a P-layer is uniform, and therefore, the photo current collected by one electrode, is inversely proportional to the distance between the incident position and the electrode in question. Two signals are given, I_1 and I_2, see figure 3.4.

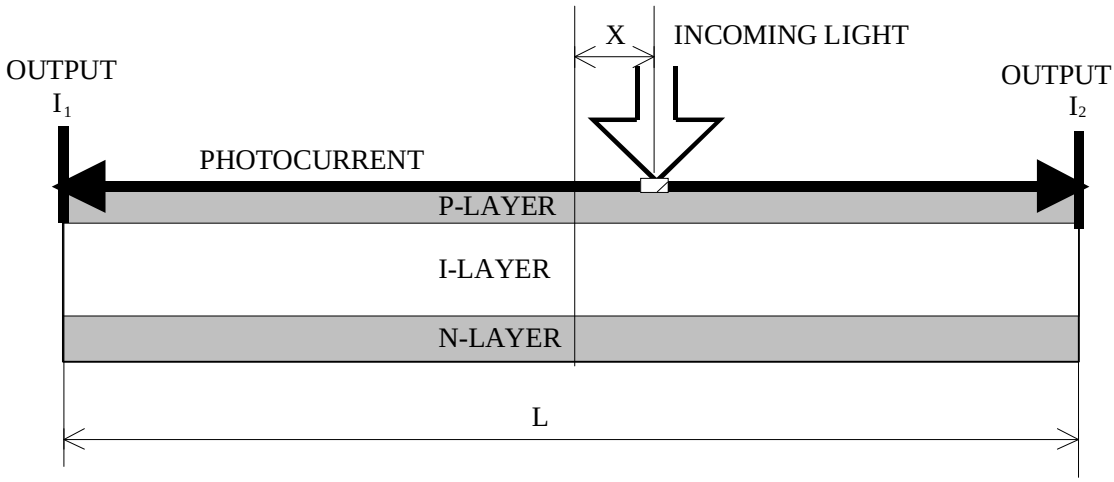

Fig 3.4: The position sensitive diode.

The position X is given by:

$$\frac{I_2 - I_1}{I_2 + I_1} = \frac{2X}{L} \qquad (3.1)$$

where the centre of the diode is set as the origin. The electric circuit for this diode includes a signal addition as well as subtraction circuit, a divider and a signal amplification device, that makes it possible to set the desired amplification (see Appendix 3A).

3.2.2 The Optical Set-up

The set-up is shown in figure 3.3 and mentioned in the introduction to this chapter. The laser is a 15 mW beam-expanded HeNe laser (λ=633 nm) with an output power of 3.5 mW after spatial filtering. This is used to focus a light spot onto the target with a planar-convex lens. The focal length is f=500 mm. Calculating the focal spot size (Eq.3.2) with a beam diameter of 25 mm yields a size of ≈20 μm on the target, and best focusing is found by looking at the speckle pattern in the scattered light from the target surface. When the speckle spots are as large as possible, the focusing is optimal.

Formula for calculating focal spot size d (Condition: $D>>d$): $d = \frac{4f\lambda}{\pi D}$ (3.2)

with f: the focal length for the lens, λ: the wavelength for the laser and D: the diameter of the e^{-1} amplitude.
The spot on the target is re-imaged with a second planar convex lens onto the PSD. In this set-up, f=190 mm is used, at a distance of about 250 mm. An aperture is introduced, close to the imaging lens, to limit the spherical aberrations that occur strongly when the whole lens diameter is used. The result is a clean sharp spot on the PSD, which is needed because a blurry spot gives a noisy signal.

3.2.3 The Piezoelectric Translation Stage

For a piezoelectric element, there is a relation between a voltage and a strain in the material. As an element in an electronic circuit, it works as a capacitor. It is characterised by an extremely good linearity and small hystereses as well as temperature independence. The hystereses is small for small voltage reversals and larger for larger voltage reversals [8]. The principle is that an electric charge, Q, is connected with a deformation of the material, ΔL, such that: $Q=K_1\Delta L$, where K_1 is a constant [9]. The material follows Hooke's law: $\sigma = E\varepsilon$, where $\sigma=F/A$ is the stress, E the elasticity module and $\varepsilon = \Delta L/L$, the strain for the material. The charge is thus proportional to the force F that induced the deformation ΔL.
The piezo electric translation stage is a stacked, low-voltage Melles-Griot 17 TFD 001/D Nano Flex single axis flexure stage with 50 μm range for piezo electric travel, according to specifications [8]. It is mounted as a base to the target and allows movement in the normal direction to the target surface. The resolution is 50 nm.
A mechanical position meter is used to measure the position changes and that showed the piezo translator to have a maximum range of 75 μm. In the following measurements and estimations, the piezo-translator is also said to have a 75 μm range (instead of 50 μm). Having this as a reference will secure the real values to be better than the measured, so this is used as a safe margin.

3.2.4 The Low-Pass Filter

The low pass filter is a simple RC-circuit, that makes it possible to set a time constant for the control, see figure 3.5. (A large capacitor and a small resistance are used to have a low impedance.) It is introduced to prevent control of noise and fast-moving position changes, coming from the target polish.

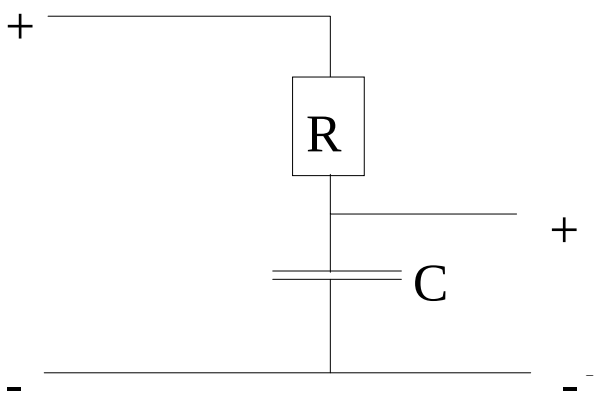

Figure 3.5: The RC-filter

3.2.5 The control equipment

The control equipment is a Satt Control ECA-40 commercial PID controller made for industrial use. The principle is that, fed with a position-related signal, the PID control unit corrects the position to the desired one [10]. It keeps the measured output signal constant, to a pre-set value. The controller has three parts; the P- part is a **P**roportional part, for which the control signal is proportional to the difference between output and pre-set reference signal. The I part is an **I**ntegrating part and has as a function to increase the control signal for as long as there is a difference between the reference signal and the output signal. The D part is a **D**ifferentiating part that is proportional to the first derivative of the output signal, i.e. it tries to predict what will happen.

The algebraic expression for the output signal is;

$$u(t) = K\left(e(t) + \frac{1}{T_I}\int_{t_0}^{t} e(\tau)d\tau + T_D \frac{d(-y(t))}{dt} \right) \tag{3.3}$$

where T_I is the integrating time, the time that the control system allows until it reaches the desired value, T_D is the differential time and K is the proportional part (dimensionless). The error, *e(t)*, is the difference between the reference signal and the measured signal;

$$e(t) = r(t) - y(t) \tag{3.4}$$

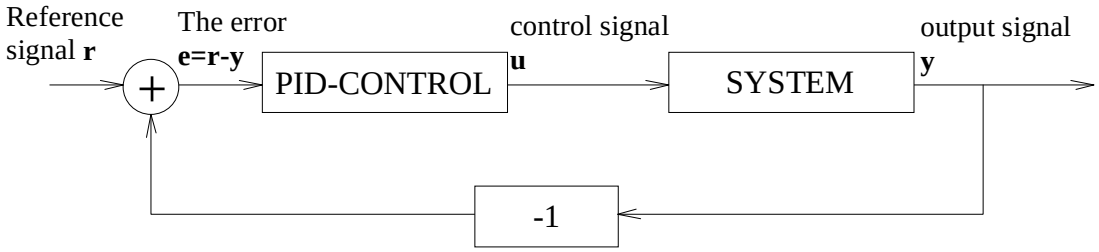

Figure 3.6 Control scheme. The "-1 box" denotes negative feedback.

When a mathematical model of the control process is known, it is possible to calculate how the parameters *K*, T_I and T_D should be set. This will give good performance for the PID controller. If the mathematical model is unknown, Ziegler-Nichol's method can be used for parameter setting. This method says that, setting the system with infinite integration time and zero derivation time (disconnecting *I*- and *D*- parts), then increase *K*, until the system becomes unstable, and starts to self-oscillate, it is possible to determine the appropriate *K*, *I* and *D* parameters. If the *K* for self-oscillation is denoted K_0 and the period time for the oscillations is denoted T_0 , Ziegler-Nichol's methods suggest a parameter setting according to table 3.2;

Controller type	K	T_I	T_D
P	0.5 K_0		
PI	0.45 K_0	T_0 /1.2	
PID	0.6 K_0	T_o /2	T_0 /8

Table. 3.2: Ziegler-Nichol's methods for setting PID parameters.

This is good as starting values, however, it is often necessary to change the parameters, while checking for changes in the output signal, and optimise the control further. In the experiments, this method is used for parameter setting.

3.3 Measurements and results

Many runs have been conducted with the set-up shown in fig 3.3 or similar, and different results have been given. Clearly, the system is very sensitive to changes in the set-up, but once fixed in the right way it can give accurate signals and response control to an acceptable degree. The sensitive factors are:

1. Focusing geometry
2. Reflection and light intensity
3. Filtering and amplification of the position signal

In the following sub-chapters, each one of these factors will be dealt with, and problems discussed according to reference signals and response control. The last subchapter, 3.3.4 Control, will present the achieved result for this set-up.

3.3.1 Focusing geometry

The smallest focus possible, was first thought to be the best, because very small movements are desired to be detected. However, a small focus on the target gives large wandering speckles in the reflected light and thus the intensity through to the diode will vary a lot. Enlarging the focus on the target results in smaller speckles and still a good resolution in the position signal. Further experiments showed that the focusing onto the target was not an important factor for resolution. It is possible to be out of focus and have small speckles and still resolve micrometer movements. Also the signal tends to get smoother for out of focus conditions. For the re-imaged focus, the important feature for achieving a good signal is that the spot falling on the PSD is a sharp spot, without blurry edges. An aperture at a distance of 3-4 cm after the imaging lens was introduced and with a numerical aperture of about NA=0.017, most of the blurriness coming from spherical aberrations disappeared. The re-imaged focus is estimated to be <100 μm diameter for smallest focus, but since best signal is achieved for out of focus conditions, the diameter is probably a lot larger, still less than 1 mm, since it has to fit into the diodes sensitive surface. There is no exact way of telling when the PSD is exactly in the re-imaged focus position, but altering the position well around the re-imaged focus does not show any particular signal change. The conclusion here is that focusing conditions for the HeNe beam is important in that

small speckles are desired, along with a small image of the focus onto the PSD (diameter <1 mm, limited by the effective area of the diode). Further quantification of these conditions is hard to make. It is basically a trial and error mission to find the required conditions for desired resolution.

3.3.2 Reflection and light intensity

The intensity of the imaged spot varies, and if this variation is large enough, this could be a source of error in the position signal. These intensity changes appear since the speckle pattern incident on the lens varies, as mentioned above. It is also induced by the reflectivity of the target surface. Experiments have been made to test the linearity of the PSD for different light intensities. The measurements were made with a LPIR laser power meter. These results show that the diode has a range where it responds linearly with a position signal, above this range it saturates and below it, it is not able to respond linearly to position changes. Changing the position for different laser powers showed that this range is roughly 1-400 μW for an estimated spot size of 50 μm (the background light was 0.04 μW over the sensitive area of the power meter ≈1 cm^2). For an unused surface of the target, not exposed to terawatt laser pulses, the reflected light is, when focused to a spot size of the same diameter, about 100 μW. When focusing on a used surface, where the terawatt-beam have made the reflectivity lower, the reflected light is not enough to achieve a reliable position signal. Intensity fluctuations for the terawatt laser exposed surface is also much larger than for the unexposed surface, which is expected, because small pits are formed in the target material by the intense laser pulses.
The target surface has a circular pattern from rotations when manufacturing the target plates, and this will affect the pattern of the reflected light as well, see figure 3.7. The origin of the different patterns is probably a mixture of diffraction and reflection. The circular line structure is well-defined with a splitting of 5-10 μm. This pattern can work as a diffraction grating for the coherent laser light and result in the observed differences. The best measuring conditions is when the pattern is elongated in the

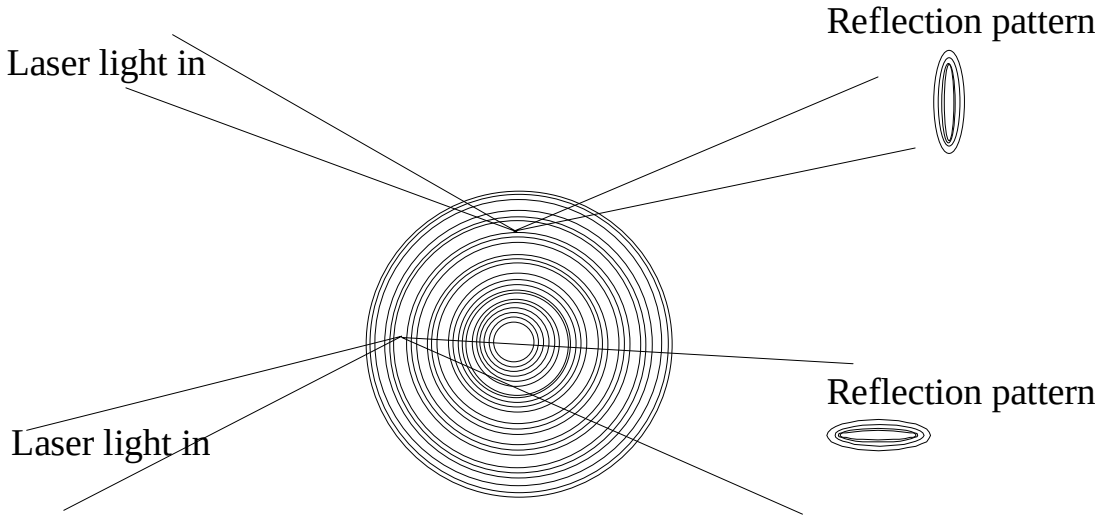

Figure 3.7: Different reflection patterns for different HeNe laser focusing positions. Upper alternative made the position signal least noisy.

vertical direction, this is when the signal from the PSD is least noisy. Therefore, focusing the HeNe beam where the target pattern is parallel to the PSD area is best for the signal conditions.
Different targets have been tried and no difference in control performance of Ta and Gd is noticed. An unused surface is desired to make the reflected light intensity high.

3.3.3 Filtering and amplification of the position signal

A low pass filtering of the position signal is made to prevent control of optical and electronic noise. Also, as mentioned earlier, the position detection cannot be made in the same place as where the terawatt laser is focused. This fact makes it crucial to dismiss position changes with a higher frequency than the one decided by the distance between the terawatt focus spot and the spot where position detection is made. A time constant of 1 second (C=2200 μF, R=560 Ω) is chosen. (The revolution speed of the target is set to ≈20 seconds)
The PSD electric circuit is equipped with a potentiometer allowing different amplification of the signal to be set. The PID controls a signal of 0-10 Volts and using this range as much as possible will increase control properties.
For small initial position changes, amplification is turned up and for larger, it is turned down. Maximum usage of a 0-10 Volt range is desired

3.3.4 Control

Setting the PID control equipment according to Ziegler-Nichol's methods, control has been shown successful down to less than 2 μm movements with an initial wobble of 12 μm, measured with the mechanically calibrated piezo translation stage (see Appendix 3B). The ratio uncontrolled/controlled signal varies slightly according to the initial wobble. Starting with 12 μm going to 2 is a factor of six in improvement. Starting from say 40 μm results in a controlled signal with 5 μm in variation, which gives a larger ratio (ratio=8). The reason for this ratio variation could be that the control parameters (K, T_I and T_D) are not fully optimised in the experiments. The achieved limit for the position control and for the experimental set-up is the one mentioned above 12-2 μm. The required position stability is a few micrometers and the result here shows the possibility of position control of the target for position variations with a lower frequency than 1 Hz.
The control parameters are set as K=2.76, T_I =2.3 and T_D =0.6. The values of the limits for best control performance seem to vary even for slight changes in the experimental set-up. This is probably because even smaller changes in the set-up induces large signal changes, and a re-calibration of both PSD and piezoelectric translation stage is required at such occasions.

3.4 Implementation in real set-up

Experiments have been made in the X-ray generation chamber where the equipment is meant to operate. There have not yet been any attempt to implement it in X-ray generation experiments. At this time, the set-up does not fit in the chamber and new lens mounts have to be designed and made, before this can happen. Also there might be a change of laser to a diode laser instead of the HeNe laser used now.
However, tests with the terawatt laser light running were conducted, and showed a few important facts:

The terawatt light found its way through to the position detection (the PSD) and limiting the disturbances from this light is obtainable in two ways:

i.) Usage of an interference filter that transmits only HeNe light. A filter with 50-60% transmission for HeNe light (633 nm) was used in this experiment and showed good performance.

ii.) Trying to re-image the terawatt laser focus outside the sensitive area of the PSD.
Focusing the HeNe at a distance from the terawatt focus, the image of the two different focus spots will not be re-imaged in the same place and it is possible to make the terawatt focus image miss the PSD and thus not substantially disturb the position measurement.

With the required changes of the optics and chamber fitting, the system shows potential to work in an X-ray generation environment. An improvement in target surface preparations (well-polished surface) is also suggested for the future.

4. The Saturable Absorber

4.1 Introduction to pre-pulse changes

The terawatt laser generates pulses of 150 fs duration. Due to leakage from the amplifiers in the laser system, 11 ns (round-trip time for regenerative amplifier) before this pulse, a pre-pulse is let out. This pre-pulse will, if it is intense enough, create an expanding plasma and decrease the high-density in the target. Doing that, it will probably change the energy distribution of the generated X-rays towards lower energies. The saturable absorber is introduced into the terawatt laser beam to make it possible to control the pre-pulse intensity. This is achieved because the saturable absorber can be made to let most of the main pulse through while it absorbs most of the pre-pulse. There is also an offset level in the laser pulse, called the ASE level. (amplified spontaneous emission) This originates from the amplifiers and will also, if it is large enough, create a plasma before the main pulse. The ASE level is also decreased by the saturable absorber. The pulse change is shown in fig 4.1 (not real measurements)

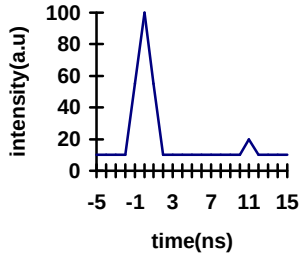

Figure 4.1a: Before saturable absorber

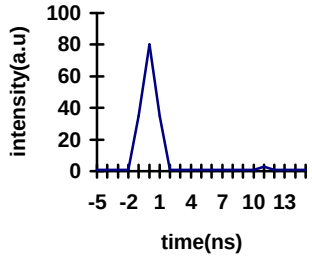

Figure 4.1b: After saturable absorber

4.1.1 The saturable absorber cell

The absorber cell is constructed by Division personnel from drawings obtained from Stanford University (see figure 4.2 and Appendix 4A). It is a large aperture (67 mm) flowing dye cell that allows a liquid to flow between two anti-reflection coated windows, separated by 4 mm. A motor driven pump flowing mechanism prevents the solution from partial heating. The liquid is a dye solution that can absorb the laser light to a certain extent, according to the concentration. Connected with the cell are four pipes, two in the bottom for inlet and two on top for outlet of the dye solution. A metal fin is sometimes introduced between the windows to minimise turbulent flow in the cell. The dye used is Exciton IR-140 diluted in methanol *pro analysi*. This dye performs well for wavelengths around 800 nm.

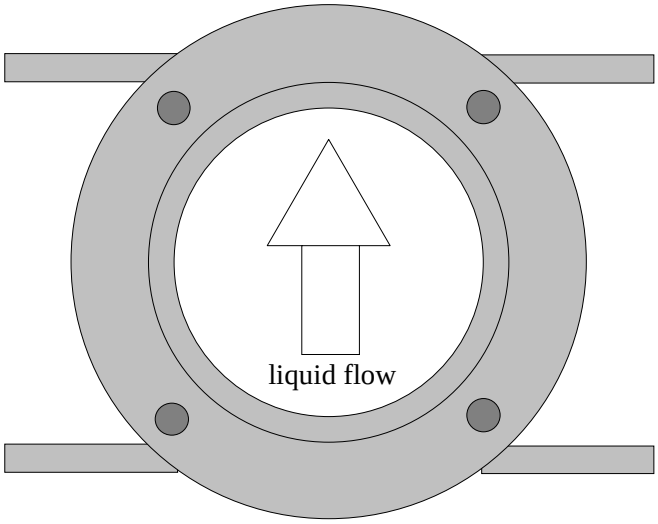

Figure 4.2: The saturable absorber cell, front view.

4.1.2 Pulse propagation through a saturable absorber

The working equation for pulse propagation through a non-linear medium such as our saturable absorber is [7]; (Derivation, see Appendix 4B)

$$T(t) = \frac{T_0}{T_0 - (T_0 - 1) \cdot exp(-U_{in}(t)/U_{sat})} = e^{-\sigma N_{tot}(t)} \qquad (4.1)$$

where $T(t)$ is the time-dependent transmission through the cell, T_0 is the pre-pulse transmission, or rather, the transmission for low intensities where no saturation of the dye is obtained. $N_{tot}(t)$ is the total number of atoms ready to absorb at a certain time and U_{in} is the energy before the cell divided by the beam diameter. U_{sat} is the saturation fluence for the medium, defined as the fluence where an atom has a 50 % chance of absorbing during a pulse time much less than the recovery time of the atom. U_{sat} is related to the absorption cross section, σ, as;

$$U_{sat} = \frac{\hbar\omega}{2^* \sigma} \qquad (3.2)$$

and knowing U_{sat} makes it possible to determine σ. (The constant $2^* \equiv 2$, see appendix 4A) Then, it is possible to calculate a certain concentration for the dye for a certain transmission and all the parameters in the equation will be mastered, since both $T(t)$, T_0 and U_{in} are measurable.

4.2 Measurements and results with the HeNe-laser

Before using the absorber cell in the terawatt beam, some tests were conducted to check if the liquid flow affected or perhaps ruined the focusing conditions, when a laser beam propagates through the cell. This is done by examining changes of a long distance focused HeNe beam. As an analyser, a CCD camera connected to a 486 PC equipped with a Videoblaster card is used, see figure 4.3. Long distance focusing is used to make the focal spot large, in which it is easy to detect small changes of focusing conditions. Two glass plates are also introduced in the beam to decrease the intensity and prevent saturation in the CCD camera. The image of the focus is analysed in a profile program that yields an intensity cross-section of the focal spot and the FWHM is measured for different flow rates. Tests were made with both water and methanol (Methanol is used as a solvent for the dye) and focal changes were detected in both vertical and horizontal directions. The focal changes did not show any correlation to the liquid flow changes, see figure 4.4. The focal spot variations occurred randomly and the conclusion here is that the flow does not create any noticeable disturbance to the focusing. No particular difference was detected with or without the fin that is supposed to make the flow non-turbulent.
However, something else noticed in these measurements is that the light spot oscillates when the flow is very slow, (slow flow is here less than 2 cm/sec). The oscillations increase in frequency and decrease in magnitude when the flow speed is increased. At a flow speed of about 3 cm/second these oscillations were no longer detectable. This suggests that the liquid should be run at a higher speed than this (7 cm/sec is chosen in our experiments). The flow rates are measured by timing the speed of small water bubbles and the error is estimated to be about 20 %.

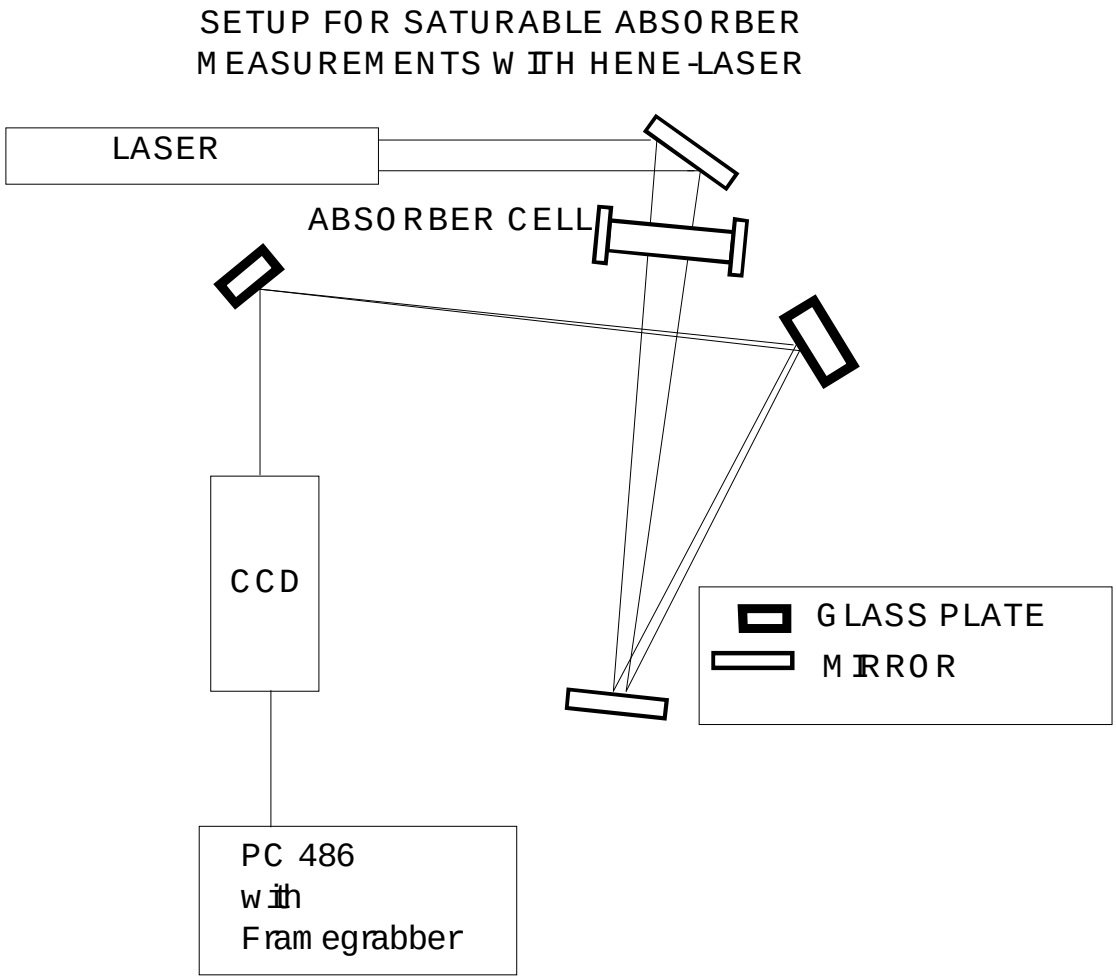

Figure 4.3: Set-up for saturable absorber measurements with the HeNe Laser

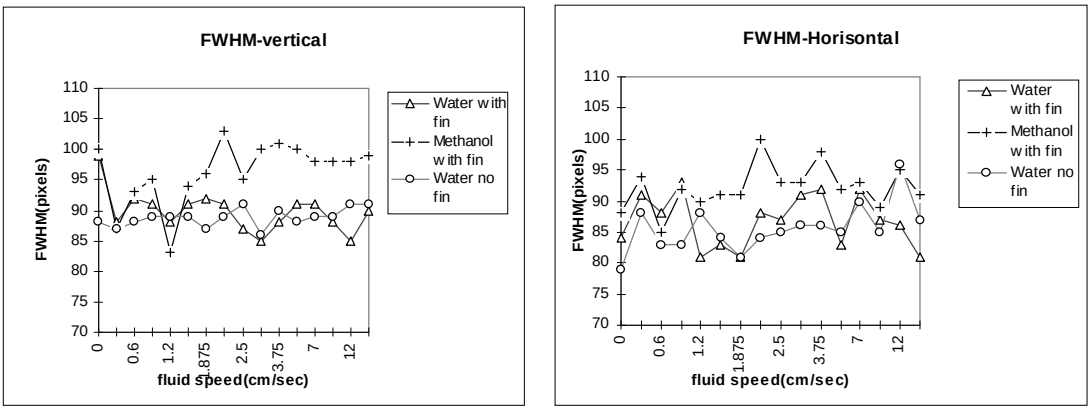

Figure 4.4 The FWHM of a HeNe focus taken with a CCD camera. No correlation between flow rate and focusing conditions is detectable.

4.3 Measurements and results with the Terawatt system

After the focusing tests in the HeNe laser system, the saturable absorber is introduced in the terawatt laser system and an analyse of the parameters in equation 4.1 is conducted. With a Hamamatsu S2839 fast laser diode and a Tektronix digital oscilloscope, it is possible to separately detect the pre-pulse and the main pulse. The detection is taken after reflection on a low-reflective surface. ND filters are also used for the main pulse, to prevent saturation of the diode. The ND filters decrease the transmission for the laser light a factor 10^x, where x is the ND factor for a certain filter. The transmission for small signals through the cell is measured as the transmission for the pre-pulse, which in comparison to the main pulse is a small signal. The time dependent transmission for the main pulse is measured as the energy fluence before passage of the cell U_{in} divided by the energy fluence out of the cell U_{out}. This is an overall or pulse averaged energy transmission after the whole pulse has passed and there is a factor of two error made by taking this as the maximum time dependent transmission (half the pulse absorbed). This is an acceptable error in the experiment, in comparison to other estimations. (The most rough estimation is probably to assume a gaussian pulse-shape of the pulses.) The energies are measured with a laser energy meter, and the error in these measurements is estimated to 10%. The measurements on the oscilloscope of the pre-pulse suffer from larger errors (estimated 20%). The ND filters have been tested with a HeNe beam and those tests showed a maximum error of 25 % in the ND factors.

Many measurements are made with the saturable absorber, for different laser energies and different concentrations of the dye. Three values are taken with constant laser energy and concentration and calculations are made with the mean values of the measurements. The result achieved is an increase in main pulse/pre-pulse ratio four orders of magnitude(10^4) for a laser energy of 85 mJ and with a 70 % transmission of the main pulse. The concentration of the dye is 0,043 mM and the beam diameter is 15 mm. The calculations of U_{sat} according to Eq.4.1 showed surprisingly good accordance between measurements with different concentration and energy. The value of U_{sat} is calculated to be between 0.6-2.9 mJ/cm^2 and with 5 out of 7 values being between 0.9-1.4 mJ/cm^2.

Another test was also conducted, where the factor 10^4 showed to be important. With only the amplifiers in the laser system turned on, and the laser-oscillator seed blocked, plasma was formed and an ND-4 filter was needed to interrupt plasma formation. This corresponds to a factor 10^4 and this is what is achieved with the saturable absorber. The ASE level is thus decreased after the saturable absorber, and cannot cause any plasma formation. Another important feature for the dye is that it showed characteristics of ageing, i.e. the absorption decreased after running the laser for a long period (hours), especially for high laser energies. This will of course be a problem for longer experiments, and no solution to this has as yet been found.

4.4 Further experiments

Further experiments with the saturable absorber will involve an examination of the energy distribution when the absorber is introduced in the terawatt beam and a comparison to the energy distribution without the absorber. Additionally, different dyes may be tested to see whether there is a dye with no ageing effect, which then will be easier to work with. If no such dye is found, quantification of the ageing for the present dye might be necessary. This will make it possible to maintain a satisfying absorption during longer periods in an experiment, by adding dye continuously.

5. Protective pellicle and X-ray transmission window

5.1 Introduction to protective pellicle and X-ray transmission window

Along with the main projects of this work, a number of smaller experiments have been made and two of them have resulted in changes in the experimental set-up. Those are a test of protection for the focusing mirror in the X-ray vacuum chamber, and a redesign of the X-ray output window flange.

5.2 Pellicle test

The target used in the vacuum chamber ablates, and particles are ejected out from it in all forward directions. The focusing mirror then becomes coated and this limits the lifetime of it, since it cannot be cleaned and the demands on the quality of focusing are very high. Something is needed between the mirror and the target, to protect the former from this coating, some sort of thin pellicle that does not affect the beam quality to much.
Different thin films have been tested for this purpose, for example nitro-cellulose film stretched on a thin metal ring. The test is conducted in a study of a large focus from a beam-expanded HeNe laser, with a CCD camera and a Videoblaster card to a 486 PC. (The same set-up and profile program as in the saturable absorber test is used, see figure 4.3. The dye cell is replaced with a pellicle). No substantial change was detectable to the focus. However, there were drawbacks with this device, since the film was difficult to mount on the metal ring, needed to be changed often, and was very fragile. The same drawbacks were met for another type of thin film, namely mylar. Mylar also turned out to work as a retarder. The reason retarders are inappropriate is that the polarisation is of importance for X-ray generation. The emitted high-energy X-ray lines originate from electrons that are driven into the target material. Thus, an E-field component perpendicular to the target surface is required and only P-polarised light carries such a component. S-polarised light oscillates along the target surface and can not contribute to such an E-field component.

The next test was conducted with thin glass pieces, used as cover-glass for microscopy. No retarder effect was detected and the focus did not decrease in quality to any noticeable extent. Even though the spot size seemed to change, the profiles gave us that the maximum intensity had not changed and the FWHM was about the same, see figure 5.1 and 5.2.

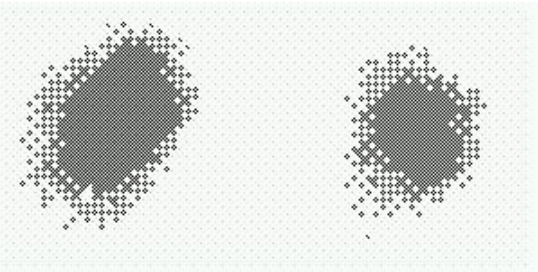

Figure 5.1: Focus spots at pellicle test. Left is without cover glass and right is with cover glass (spot size≈2 mm.)

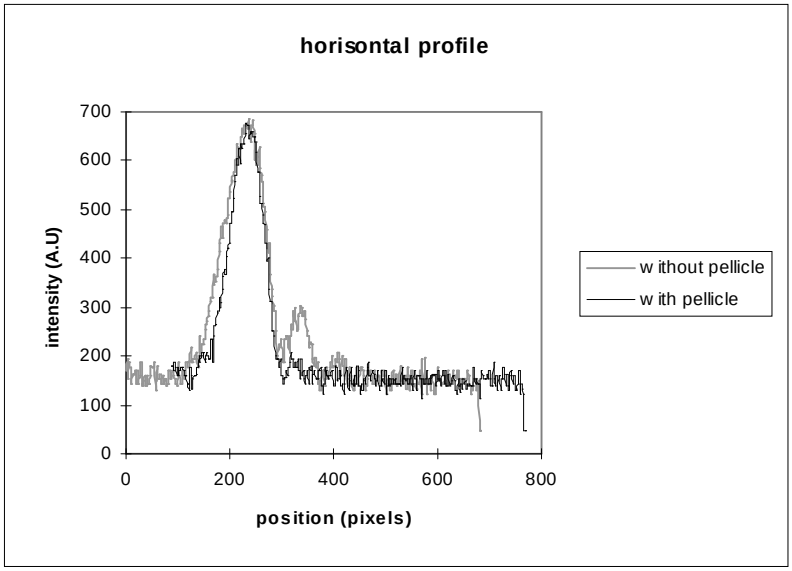

Figure 5.2a: Focus profile horizontal (spot size≈2 mm.)

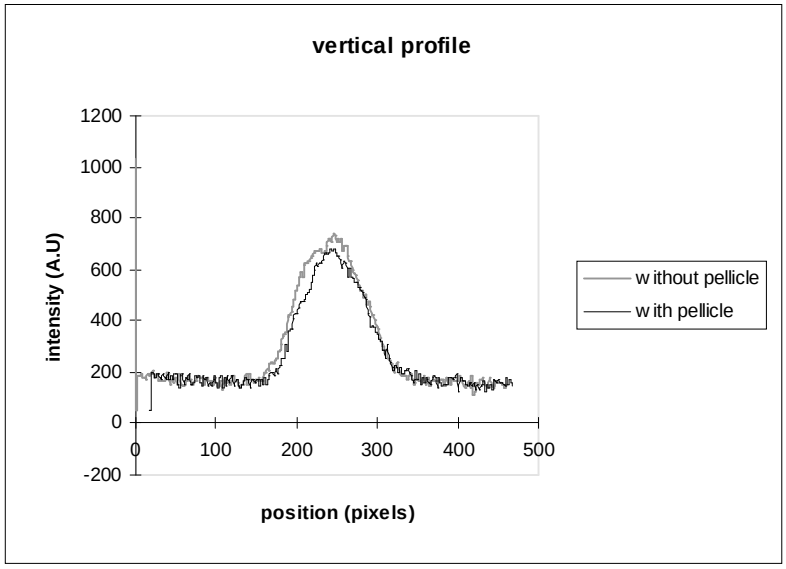

Figure 5.2b: Focus profile vertical (spot size≈2 mm.)

The result leads to the conclusion that it is possible to use these cheap, easy-changeable cover-glass plates as protection for the mirrors, without loosing much effect in the generation of the plasma. The gain is in the end, a cheaper X-ray production, since the lifetime of mirrors is increased.
The results of this method of protecting the focusing mirror have shown very successful in experiments. There is an automatic change device for the glass plates under construction that will allow a change of glass plate with vacuum kept in the chamber. This will help to keep the number of experiment interrupts to a minimum.

5.3 Changes in the chamber

For magnification imaging, it is desirable to have the object close to the plasma source and to place the imaging plate far away. This implies a necessity of moving the objects into the vacuum chamber, and the size of the X-ray output window will become important. For this purpose a larger X-ray exit window is designed, that allows a larger angle for the output X-rays. Just by re-designing the exit window flange, it was possible to increase the output diameter from 65 to 130 mm. Improvements are also made in the mounting device of the thin plastic film that serves as the X-ray exit of the vacuum chamber. The film is secured between two O-rings and with a bevelled immersion to squeeze it in place.

6. Summary

One of the aims of this diploma work was to supply control to a rotating target and to keep the target surface in focus with an allowed variation of a few micrometers. This was accomplished for a laboratory set-up, for position changes below 1 Hz. The next step in this project, is to implement the control set-up in the vacuum chamber.
Next, evaluation of a saturable absorber for pre-pulse control, or rather for pre-pulse elimination was conducted. The experiments showed great possibilities for pre-pulse control. The main pulse/pre-pulse ratio was increased four orders of magnitude with an energy throughput of about 70 %.
Tests of protection for the gold-coated parabolic mirror were conducted. The protection is needed to avoid target dust, emitted when plasma generation is in process, to coat the mirror. The result here is that cheap cover glass, ordinarily used for microscopy, could be employed without severe loss of the focusing conditions.
Re-designing the X-ray output port flange allowed a larger angle of X-rays to be used in the experiments, which is a gain both in time and economy.

The methods presented in this work are of course, as in most situations, not the only solutions to the problems. As for the position control, the possibility of using some electronic detection equipment has been on my mind during the work. The drawback with, for example a capacitive or an inductive position detection, is that with such equipment, an even larger area of the target must be used. For this type of position detection it is hard to get close to the terawatt focus spot. Even if the same problems occur in our situation, where we now cannot measure in the same spot as we fire the terawatt laser, the potential of doing the position control better does not exist with an electronic device. With the optical measurement, this possibility exists, and that encouraged us to continue the experiments on our optical set-up, despite the troubles. The structure on the target is of course another source to bad focusing and some sort of target preparation is suggested to make the target surface more smooth than it is now.

Using the saturable absorber for pre-pulse reduction is also just one way to analyse the effects induced by a pre-pulse. Some workers believe the pre-pulse to be important for a good plasma generation, and even if this is the case, control of the main pulse/pre-pulse ratio is still desired for optimisations. A frequency doubling crystal may also be used for this purpose, but here only about 40% of the main pulse energy may be doubled. The choice of a good pre-pulse reducer is dependent on what wavelength regime is of interest. For wavelengths in the micrometer regime, dye cells have a lower performance than frequency doubling crystals, but for our case (λ=794 nm), it performs well.

Appendices

Appendix 3A: The Electric circuit for the PSD, position sensitive detector

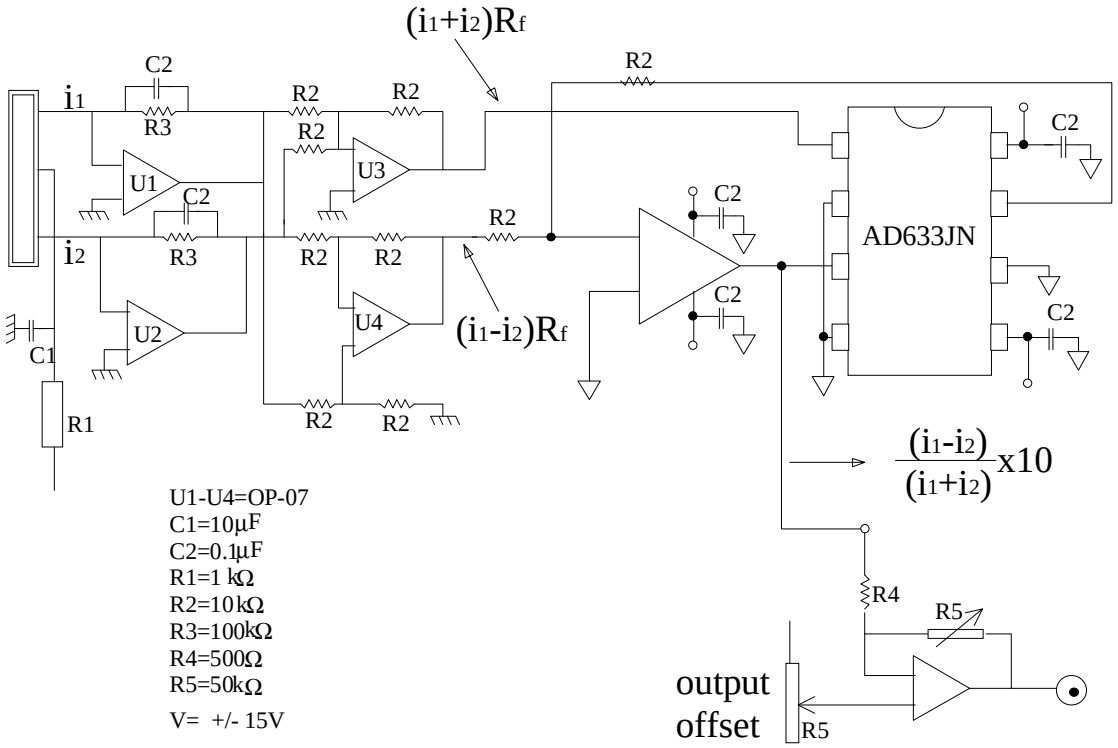

The electric circuit for the PSD with addition, subtraction and divider circuit.

Appendix 3B. Position control results, plot curve

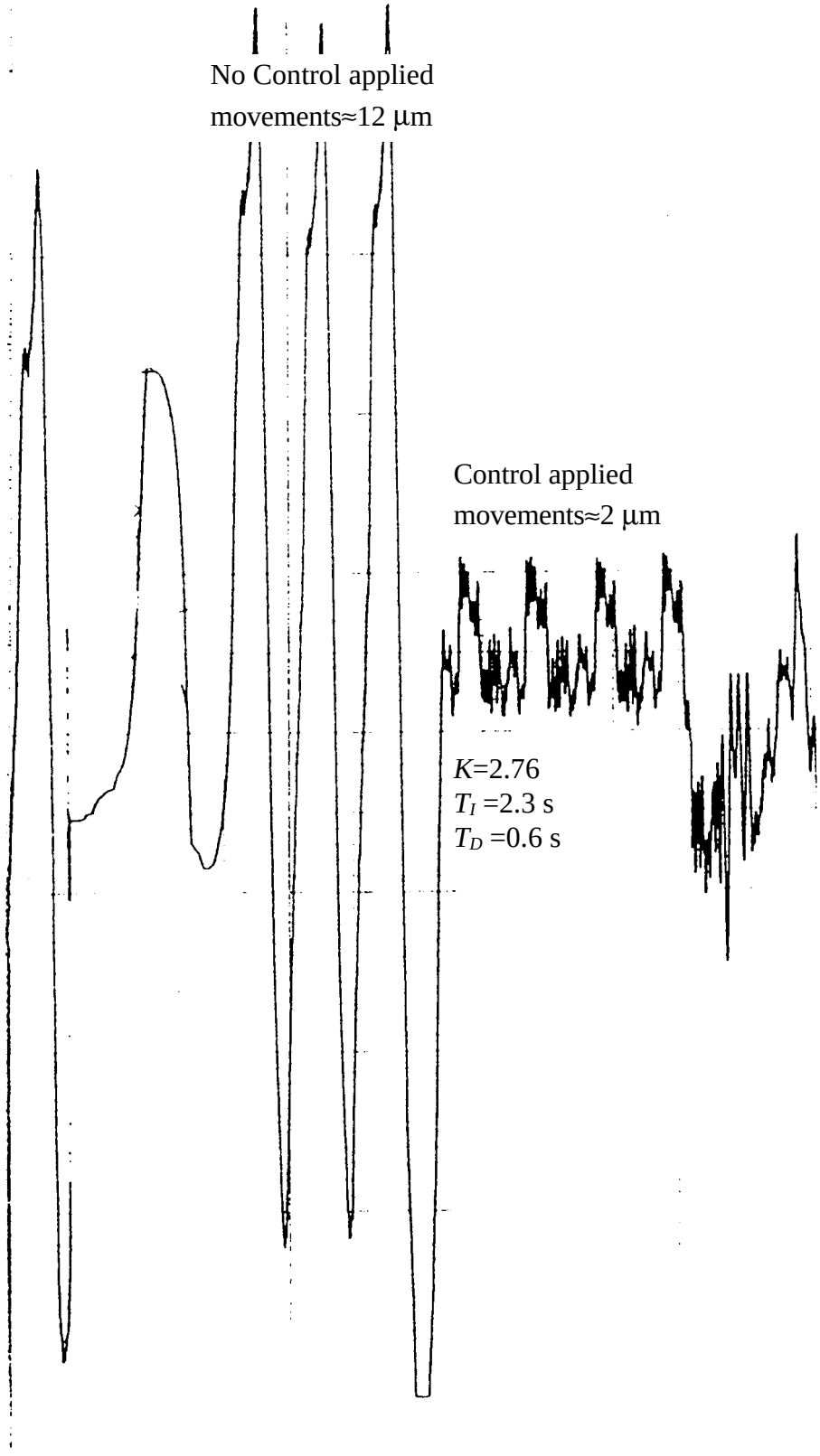

The plot curve shows the position fluctuations of the target, controlled and without control. The PID parameters are; K=2.76,T_I =2.3 s, T_D =0.6 s.

Appendix 4A. The saturable absorber cell

Drawings made at the Division of Atomic Physics, Lund. Original from Stanford University (J. D Kmetec and J. J Macklin).

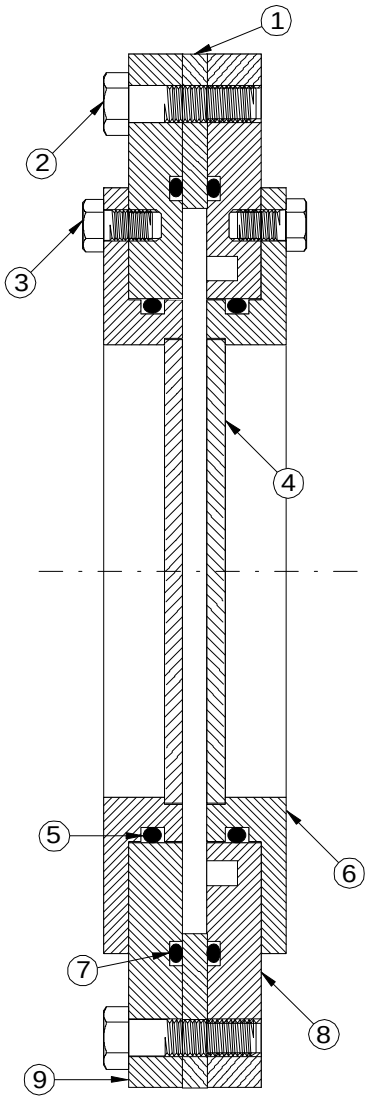

9	1	Flange #1	Stainless steel	-
8	1	Flange #2	Stainless steel	-
7	2	O-Ring	Viton	124.5 x 3 mm
6	2	Window mount	Stainless steel	-
5	2	O-Ring	O-Ring	84.5 x 3 mm
4	2	CVI Window	Glass	3" x 3 mm
3	6	M5-Screw	-	ca 8 mm
2	6	M6-Screw	-	ca 20 mm
1	1	Distance plate	Stainless steel	-

Appendix 4B: Pulse propagation through a non-linear medium.

Derivation from [7].

Consider a pulse with a signal intensity *I(z,t)* in a moving coordinate system, travelling in the positive *z*-direction through a non-linear medium. Let *N(z,t)* be the number of atoms ready to absorb and σ the absorption cross section. It is then possible to express the intensity and the number of atoms in two differential equations;

$$\frac{\partial I(z,t)}{\partial t} = -\sigma\, N(z,t) I(z,t) \tag{4B.1}$$

and

$$\frac{\partial N(z,t)}{\partial t} = \frac{2\sigma}{\hbar\omega} N(z,t) I(z,t) \tag{4B.2}$$

Integrating 4B.1 over the length of the non-linear medium, *L*, will give

$$\int_{I=I_{in}(t)}^{I=I_{out}(t)} \frac{dI}{I} = -\sigma \int_{z=0}^{z=L} N(z,t)dt = -\sigma\, N_{tot}(t) \tag{4B.3}$$

which will become

$$I_{out}(t) = I_{in}(t) e^{-\sigma N_{tot}(t)} = T(t) I_{in}(t) \tag{4B.4}$$

where $I_{in}(t)$ is the input intensity at the input plane of the active volume and $I_{out}(t)$ is the corresponding output intensity for the output plane. The integral on the right hand side of equation 4B.3 is called $N_{tot}(t)$ for simplicity.

$$N_{tot}(t) = \int_{z=0}^{z=L} N(z,t)dz \tag{4B.5}$$

The second equation, 4B.2 integrated becomes

$$\frac{\partial}{\partial t} \int_{z=0}^{z=L} N(z,t)dz \equiv \frac{dN_{tot}(t)}{dt} = -\left(\frac{2}{\hbar\omega}\right) \int_{z=0}^{z=L} \frac{\partial I(z,t)}{\partial z} dz \tag{4B.6}$$

which can be written

$$\frac{dN_{tot}(t)}{dt} = -\frac{2}{\hbar\omega}\left[I_{out}(t) - I_{in}(t)\right] \tag{4B.7}$$

This will be the same as saying that $N_{tot}(t)$ is condensed to an arbitrarily thin slab, in which everything seems to happen simultaneously. $N_{tot}(t)$ is here to be considered as a population integrated over the total space (or time-integrated) seen by any one small segment of the pulse centred at time *t*, as that segment passes through each plane *z*. Suppose that the initial $N_{tot}(t)$ is N_0 , then the initial pass transmission T_0 will be $T_0 = exp\text{-}(N_0\sigma)$. The signal energies per unit area $U_{in}(t)$ and $U_{out}(t)$ are defined as

$$U_{in}(t) = \int_{t_0}^{t} I_{in}(t)dt \qquad (4B.8)$$

and

$$U_{in}(t) = \int_{t_0}^{t} I_{out}(t)dt \qquad (4B.9)$$

The saturation fluence is defined as the fluence for which there is a 50 % chance that an atom will absorb, if the pulse length is much shorter than the atom's recovery time.

$$U_{sat} = \frac{\hbar\varpi}{2^{*}\sigma} \qquad (4B.10)$$

where 2^{*} denotes a "saturation factor". This factor $2^{*}\equiv 1$ if the lower energy level in the absorbing medium empties out rapidly compared to the pulse duration; but $2^{*}\equiv 2$ if the lower level population accumulates or "bottlenecks" during the pulse.
U_{sat} is the pulsed analogue to the saturation intensity for continuous pulses.

U_{in} can now be rewritten as

$$U_{in} = U_{sat} \cdot ln\left[\frac{1 - 1/T_0}{1 - 1/T(t)}\right] \qquad (4B.11)$$

and U_{out} becomes

$$U_{out} = U_{sat} \cdot ln\left[\frac{T_0 - 1}{T(t) - 1}\right] \qquad (4B.12)$$

where T_0 is the transmission for small signals.

Rewriting the expression for $T(t)$ as the working equation yields

$$T(t) = \frac{T_0}{T_0 - (T_0 - 1)\cdot exp(-U_{in}(t)/U_{sat})} = e^{-\sigma N_{tot}(t)} \qquad (4B.13)$$

With this equation, it is possible to calculate the transmission for a certain absorbing medium or to calculate how an absorber should be constructed, (what concentration of absorber that is needed) for a certain requested output pulse.

Acknowledgements

This report is the result of the time spent at the Division of Atomic Physics, Lund Institute of Technology, in Sweden.
I want to thank Ian Mercer and Carl Tillman for being my advisors during this diploma work. I would also like to thank Lennart Andersson at the division of Automatic Control, who worked with me on the position control and supplied the requested knowledge and equipment. Many others of the Atomic Physic Division co-workers provided me with a physical insight when lack of such occurred, and I want to thank all of them as well, especially Anders Persson for several consultations and Sune Svanberg for being my examiner.

References

1. Herrlin, G. Svahn, C. Olsson, C. Tillman, H. Pettersson, A. Persson, C.-G. Wahlström, and S. Svamberg, *Generation of X-rays for Medical Imaging by High-Power Lasers: Preliminary Results*, Radiology. **189**, 65, (1993)

2. D. Kmetec, *Ultrafast laser generation of hard X-rays* (Thesis, Stanford University, 1992)

3. Carroll and E. T. Kennedy, *Laser Produced Plasmas*, Contemp. Phys. **22,** 61, (1981)

4. Stix, *The theory of plasma waves*, (McGraw-Hill, New York 1962)

5. Coffey, *Breaking of large amplitude plasma oscillations*, Phys. Fluids. **14**, 1402, (1971)

6. Svanberg, J. Larsson, A. Persson, and C.-G. Wahlström, *Lund High-Power Laser Facility - Systems and first results*, Phys. Scripta. **49**, 187, (1994)

7. Siegman, *Lasers* (University Science Books, Mill Valley, California 1986)

8. Nanopositioning Guide, 1993 MELLES GRIOT (Distributed by Melles Griot)

9. Grahm, H.-G. Jubrink, and A. Lauber, *Modern Industriell Mätteknik 1991, Givare*, (Bokförlaget Teknikinformation, Linköping 1990)

10. Glad and L. Ljung, Reglerteknik,-Grundläggande teori (Studentlitteratur, Lund, 1989)

General references (not referred to in the text)

S. Borgström, *Laserteknik*, (KF Sigma, Lund 1993)

E. Hecht, Optics, (Addison Wesley, Reading Massachusetts 1987), 2:nd ed.

J. D. Kmetec, C.L. Gordon,III, J.J. Macklin, B.E. Lemoff, G.S. Brown, and S.E. Harris, *MeV X-ray Generation with a Femtosecond Laser*, Phys. Rev. Letters. **68**, 1527, (1992)

M.M. Murnane, H.C. Kapteyn, and R.W. Falcone, *High-Density Plasmas Produced by Ultrafast Laser pulses*, Phys. Rev. Lett. **62**, 155, (1989)

S.-G. Pettersson and S. Borgström, *Optisk Teknik* (KF Sigma, Lund 1993)

D. Cremers and L. Radziemski, *Laser induced plasmas and Applications*, (Marcel-Dekker, New York 1989)

S. Svanberg, *Atomic and molecular spectroscopy, basic aspects and applications,* (Springer Verlag, Berlin, New York 1992) 2:nd ed.